An Asymmetry in the IOD and ENSO Teleconnection Pathway and Its Impact on Australian Climate

WENJU CAI, PETER VAN RENSCH, AND TIM COWAN

CSIRO Wealth from Oceans National Research Flagship, and CSIRO Water for a Healthy Country Flagship, CSIRO Marine and Atmospheric Research, Aspendale, Victoria, Australia

HARRY H. HENDON

Centre for Australian Weather and Climate Research, Bureau of Meteorology, Melbourne, Victoria, Australia

(Manuscript received 7 September 2011, in final form 27 March 2012)

ABSTRACT

Recent research has shown that the climatic impact from El Niño–Southern Oscillation (ENSO) on middle latitudes west of the western Pacific (e.g., southeast Australia) during austral spring (September–November) is conducted via the tropical Indian Ocean (TIO). However, it is not clear whether this impact pathway is symmetric about the positive and negative phases of ENSO and the Indian Ocean dipole (IOD). It is shown that a strong asymmetry does exist. For ENSO, only the impact from El Niño is conducted through the TIO pathway; the impact from La Niña is delivered through the Pacific–South America pattern. For the IOD, a greater convection anomaly and wave train response occurs during positive IOD (pIOD) events than during negative IOD (nIOD) events. This ''impact asymmetry'' is consistent with the positive skewness of the IOD, principally due to a negative skewness of sea surface temperature (SST) anomalies in the east IOD (IODE) pole. In the IODE region, convection anomalies are more sensitive to a per unit change of cold SST anomalies than to the same unit change of warm SST anomalies. This study shows that the IOD skewness occurs despite the greater damping, rather than due to a breakdown of this damping as suggested by previous studies. This IOD impact asymmetry provides an explanation for much of the reduction in spring rainfall over southeast Australia during the 2000s. Key to this rainfall reduction is the increased occurrences of pIOD events, more so than the lack of nIOD events.

1. Introduction

Tropical sea surface temperature (SST) variations associated with El Niño–Southern Oscillation (ENSO) drive both tropical and extratropical responses. The baroclinic response to the diabatic (convective) heating anomalies induced by the tropical SSTs leads to a hemispheric-wide, tropically trapped pattern resembling the Southern Oscillation (SO) (e.g., Gill 1980). The same diabatic heating also excites equivalent barotropic Rossby wave trains, such as the Pacific–South America (PSA) pattern that emanates from the tropics to the extratropics (e.g., Hoskins and Karoly 1981). A recent study highlighted the extratropical impacts of the Indian Ocean dipole (IOD) that are conducted through similar pathways to ENSO during austral winter and spring (Cai et al. 2011). Diabatic heating anomalies from the west and east poles of the IOD generate Rossby wave trains, referred to as the western and eastern Indian Ocean Rossby wave trains, respectively. The two wave trains appear to share a pressure anomaly center south of Australia, which strongly influences the climate in the surrounding regions (e.g., southeast Australia). The finding reinforces earlier results of an IOD impact on remote regions through such equivalent barotropic Rossby wave trains (Saji and Yamagata 2003b; Ashok et al. 2007; Chan et al. 2008; Cai et al. 2009b).

During the austral spring season [September–November (SON)], the teleconnection from ENSO to regions such as southeast Australia stems primarily from these wave trains emanating from the covarying SSTs associated with the IOD in the tropical Indian Ocean (TIO) (Cai et al. 2011). This is because the tropical response to the

Corresponding author address: Wenju Cai, CSIRO Marine and Atmospheric Research, PMB 1, Aspendale VIC 3195, Australia.
E-mail: wenju.cai@csiro.au

DOI: 10.1175/JCLI-D-11-00501.1

ENSO–SST anomaly in the equatorial Pacific is confined to tropical regions such as northeastern Australia, and it does not extend to southern Australia. Additionally, the anomalies of the PSA, which result from the Rossby waves forced by the SST anomalies in the central Pacific, are located too far east from Australia with no pathway to influence southern Australia. In other words, the impact of ENSO on southern Australia in SON tends to be conducted through the TIO via Rossby wave trains. This means that the teleconnective impact of the IOD dominates that of the ENSO in terms of the climate over southern Australia, because the impact from El Niño relies on covarying conditions in the TIO to convey its signal.

Cai et al. (2011) assumed a linear relationship when examining the teleconnections, with symmetrical contributions from El Niño and La Niña events. However, it remains unclear if the extratropical teleconnection of ENSO via the TIO is symmetric. Adding to this is the question of the IOD's impact—is it symmetric with respect to its positive IOD (pIOD) and negative IOD (nIOD) phases? These issues require clarification, which will help in understanding some of the dynamics behind the 2002–09 austral spring rainfall reduction over southeast Australia. For example, is the rainfall reduction due to a lack of nIOD events (Ummenhofer et al. 2009) or does it stem from an increase in pIOD events (Cai et al. 2009b)? If the impact is asymmetric, then these two interpretations would be rather different.

The possibility of an asymmetrical IOD impact is raised through the fact that an amplitude asymmetry already exists between the positive and negative phases of the IOD and ENSO. Studies have noted that the SST variance in the east pole of the IOD (IODE) is far greater than that in the west pole (IODW) (Saji and Yamagata 2003b; Hong et al. 2008), and that maximum negative IODE SST anomalies can grow far greater than the positive anomalies; this is manifested as a negative skewness in IODE SST anomalies, thereby resulting in producing a positive skewness in the IOD, as the dipole is defined as the difference between the western and eastern poles (Saji et al. 1999). However, the relative contribution from various processes to the production of the positive skewness of the IOD is not clear. Possible processes include nonlinear temperature advection, a SST–cloud–radiation feedback, and feedbacks between the thermocline, SST, and wind. Likewise, the amplitude of El Niño is significantly larger than the amplitude of La Niña (Hoerling et al. 1997; Burgers and Stephenson 1999; Jin et al. 2003; An and Jin 2004). As with the IOD, the cause of this ENSO positive skewness is still an open question. The positive skewness of ENSO SST anomalies may partly contribute to the positive skewness of the IOD because El Niño and pIOD often develop concurrently. Linearly removing ENSO from the IOD reduces the IOD skewness to below significant values, but this does not confirm that ENSO is the sole cause of the IOD skewness, due to the high ENSO–IOD coherence. Using another method Hong et al. (2008) suggest that the IOD skewness in the dominant eastern pole still exists after the ENSO skewness is removed.

Regardless of how the positive skewness of the IOD and ENSO comes about, it is an open question as to whether this positive skewness in the IOD and ENSO generates an asymmetric response in circulation anomalies. What are the implications for rainfall teleconnections across tropical and extratropical regions (such as southern Australia in SON)? We examine these issues, the associated mechanisms, and the implications on regional rainfall variability and changes.

2. Data and method

We focus on data from 1950 to 2009 rather than from during the post-1979 satellite era to allow for more samples of positive and negative phases of ENSO and the IOD. We also restrict our analysis to SON, as this is when ENSO and the IOD strongly covary and have a significant influence on Australia's climate. The analysis utilizes Met Office Hadley Centre Global Sea Ice and SST (HadISST) reanalyses (Rayner et al. 2003) to monitor tropical SST variability. ENSO is described using the Niño-3.4 SST index (average SST anomalies over 5°S–5°N, 170°–120°W), while the IOD is described through a dipole mode index (DMI; Saji et al. 1999), defined as the difference of the area mean SST anomalies in the IODW region (10°S–10°N, 50°–70°E) and the IODE region (10°S–equator, 90°–110°E). Associated variations in deep tropical convection and circulation anomalies are diagnosed using the mean outgoing longwave radiation (OLR), geopotential height at the 200-hPa level (Z200), and upper-level divergence, from the National Centers for Environmental Prediction–National Center for Atmospheric Research (NCEP–NCAR) reanalyses (Kalnay et al. 1996). Deficiencies have been observed when comparing these fields between various reanalysis products, with no single reanalysis product proving more reliable (Newman et al. 2000). However, there is a general agreement between the fields within individual reanalysis products, which should prove useful, at least for understanding the dynamics contained within a single reanalysis product. A gridded (0.25° grid) analysis of Australian rainfall based on available station data, subjected to extensive quality control from the Australian Bureau of Meteorology (Jones et al. 2009), is employed to examine the relative impact of IOD and ENSO phases on Australian rainfall.

An important issue is whether the relationship between SST and rainfall anomalies over the IODE region is linear. The rainfall–IODE SST asymmetry was initially examined by Hong and Li (2010) using outputs from version 2.0.2 (v2.02) of the Simple Ocean Data Assimilation (SODA) project, forced by 40-yr European Centre for Medium-Range Weather Forecasts Re-Analysis (ERA-40) wind and heat fluxes (Carton and Giese 2008). To test and verify their results, we also use SST from SODA v2.0.2, along with rainfall from ERA-40, NCEP–NCAR reanalyses, and version 2 of the Global Precipitation Climatology Project (GPCP) monthly precipitation analysis (Adler et al. 2003). The use of multiple SST and rainfall products reduces the biases and uncertainty in our results.

The basic analysis technique used in this study is linear regression (or equivalently, correlation). Unless otherwise stated, all data are linearly detrended to ensure that any relationship that is produced is not a result of long-term trends in the respective time series. Regression coefficients (and the corresponding correlations) are first calculated by regressing anomalous circulation fields onto Niño-3.4 and the DMI using all samples (assuming a symmetric response with respect to positive and negative phases). Regression coefficients are then calculated using samples containing only positive (El Niño or pIOD) and negative index (La Niña and nIOD) values. The corresponding correlations are also calculated and, where possible, indicate the statistical significance at the 95% confidence level. A comparison of the regression coefficient patterns, in terms of a per unit change of the positive and negative index values, is then made, so as not to be influenced by the amplitude skewness of each index. Sensitivity tests were also performed to determine the strength of using this regression method, particularly the sensitivity when samples with values close to zero are excluded. Results show that the asymmetry remains.

3. Evidence of an asymmetry in ENSO impacts

We first focus on the extratropical impact of ENSO conducted through the TIO using all samples. If we assume a symmetric circulation response to positive and negative phases of ENSO (Cai et al. 2011), then the ENSO–IOD relationship is indeed strong with a correlation coefficient of 0.62 for the period 1950–2009 (black line, Fig. 1a). The issue regarding the relationship between the IOD and ENSO has been vigorously debated. The consensus is that while both ENSO and the IOD can force each other, the IOD can also operate independent of ENSO (Saji and Yamagata 2003a; Li et al. 2003; Kug and Kang 2006; Behera et al. 2006; Cai et al. 2009a; Luo et al. 2010). The present study will not add to this debate.

The Cai et al. (2011) study restricted its analysis to all samples, and it did not focus on any asymmetry in the impact from ENSO. Figure 1a shows the coherence between the pIOD and El Niño is much higher than that between nIOD and La Niña, indicating a potentially greater impact from El Niño compared to La Niña. La Niña events tend to occur with nIODs; however, a stronger La Niña is not strongly associated with a stronger nIOD, as shown using samples with negative Niño-3.4 values. This is true with respect to the eastern and western poles of the IOD (Figs. 1b and 1c). By contrast, El Niño events are closely linked to pIODs, with a correlation statistically significant above the 99% confidence level. This ENSO–IOD ''coherence asymmetry'' is also observed in each of the IOD poles (Figs. 1b and 1c), both significantly correlated with El Niño above the 99% confidence level. However, exceptions do exist, such as during years 2007 and 2008 when a pIOD occurred in conjunction with a La Niña (Cai et al. 2009c). Nevertheless, over the 60-yr time frame, El Niño and pIOD events tend to be coherent from a statistical viewpoint. It is not clear to what extent the high coherence is contributed to by the positive skewness of ENSO, or the positive skewness of the IOD.

Based on the regression using all samples (Fig. 2a), the tropically trapped baroclinic response to diabatic heating (convective) anomalies is manifested as positive height anomalies over the tropics. First, this is associated with anomalously low rainfall over northern Australia, as this region directly experiences anomalous sinking motion as a result of the negative SST anomalies over the western Pacific (Cai et al. 2011): this forms part of the well-known SO pattern. Second, an eastern Indian Ocean (EIO) and a western Indian Ocean (WIO) Rossby wave train, in response to convection (OLR) anomalies over the IOD poles, share a high pressure/height anomaly center south of Australia. This high pressure center reduces the intensity and frequency of the westerly rainfall bearing weather fronts, and as such is associated with anomalously low rainfall over southern Australia in SON. In the south Pacific, Rossby wave trains generated by tropical Pacific SST anomalies (referred to as the PSA) are evident, but they exist too far eastward of Australia to impact its southern regions. Cai et al. (2011) showed that some of the wave train signals south of Australia are forced by a component of the IOD that is independent from ENSO.

The stronger El Niño–pIOD coherence suggests that the extratropical impact of El Niño via the TIO is likely to be greater and more systematic than that of La Niña. This is indeed the case as shown in the regression patterns

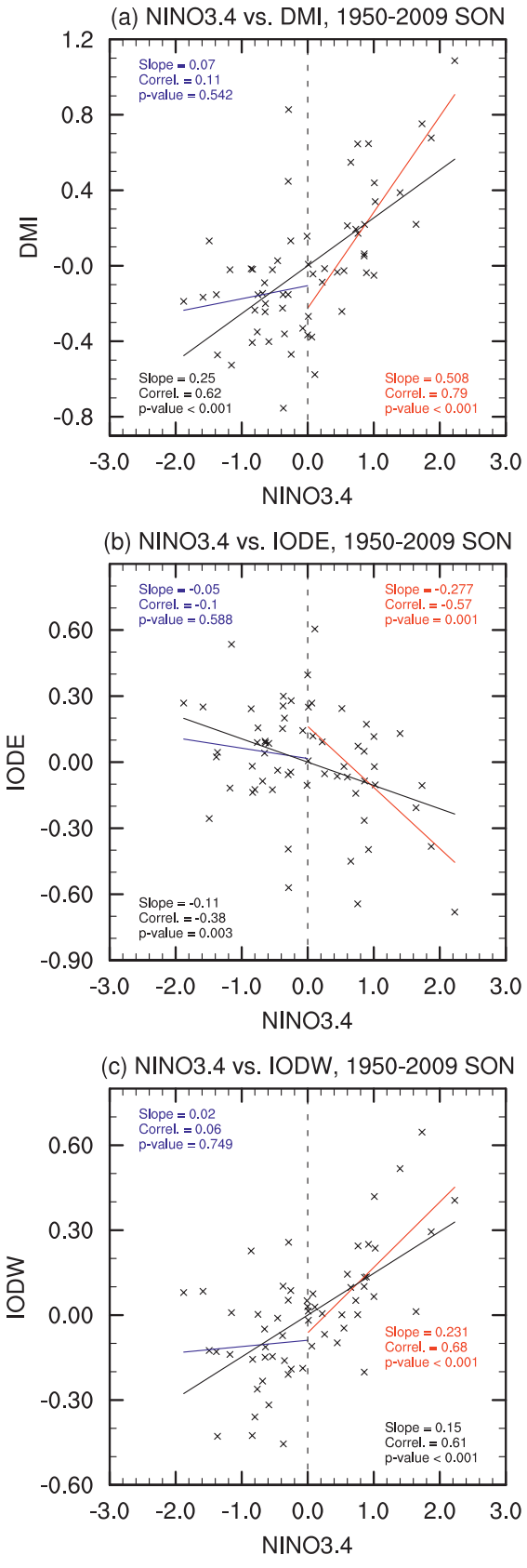

associated with positive (Fig. 2b) and negative (Fig. 2c) Niño-3.4 values. A comparison of the OLR patterns associated with El Niño and La Niña confirms the high coherence of an El Niño with a pIOD with strong subsidence over the IODE region. It is the high El Niño–pIOD coherence that is mainly responsible for the EIO and WIO wave trains seen in the middle panel of Fig. 2a.

The absence of a La Niña–induced OLR signal in the TIO is consistent with the lack of a significant wave train response emanating from the TIO, although a PSA pattern is evident in the South Pacific sector (middle panel, Fig. 2c). As such, the La Niña's impact does not go through the TIO, consistent with a lack of coherent OLR anomalies in the east TIO (left panel, Fig. 2c). Instead, the impact is delivered through a tropically trapped response and a La Niña–induced PSA pattern, which is rather different from that associated with El Niño: maximum negative OLR anomalies associated with La Niña are situated farther westward (170°E–160°W) (Figs. 2b and 2c, left panels), closer to the west Pacific and hence closer to eastern Australia, than those associated with the El Niño–induced PSA (Figs. 2b and 2c, middle panels). Because northern Australia (north of 22°S) is directly under the influence of western Pacific convection anomalies, the La Niña–induced convection anomalies enhance rainfall over much of the region. Farther south, the low pressure anomaly of the PSA enhances the rain-bearing easterly weather systems, leading to increased rainfall over eastern Australia (south of 27°S). However, the region between 22° and 27°S experiences offshore flows, with little rainfall teleconnection, marking the separation of the tropical and extratropical rainfall response. Thus, any El Niño–induced rainfall reduction across southeast Australia is conducted through the TIO, but the La Niña–induced rainfall increase comes straight from the extratropical PSA response, not through the TIO (Figs. 2b and 2c, right panels). This regional and asymmetric impact has not been brought out in the conventional linear ENSO–rainfall teleconnection analysis (e.g., Ropelewski and Halpert 1987; Cai et al. 2011).

←

FIG. 1. Scatterplot of linearly detrended (a) DMI, (b) SST anomalies over the IODE, and (c) SST anomalies over the IODW vs linearly detrended Niño-3.4 for austral spring (SON). Three sets of linear regressions are carried out: using all samples, implying a linear relationship (black); samples with positive Niño-3.4 values (red); and samples with negative Niño-3.4 values (blue). The slope, correlation, and *p*-value are shown. Linear regression coefficients with values of *p* less than 0.05 indicate statistical significance at the 95% confidence level.

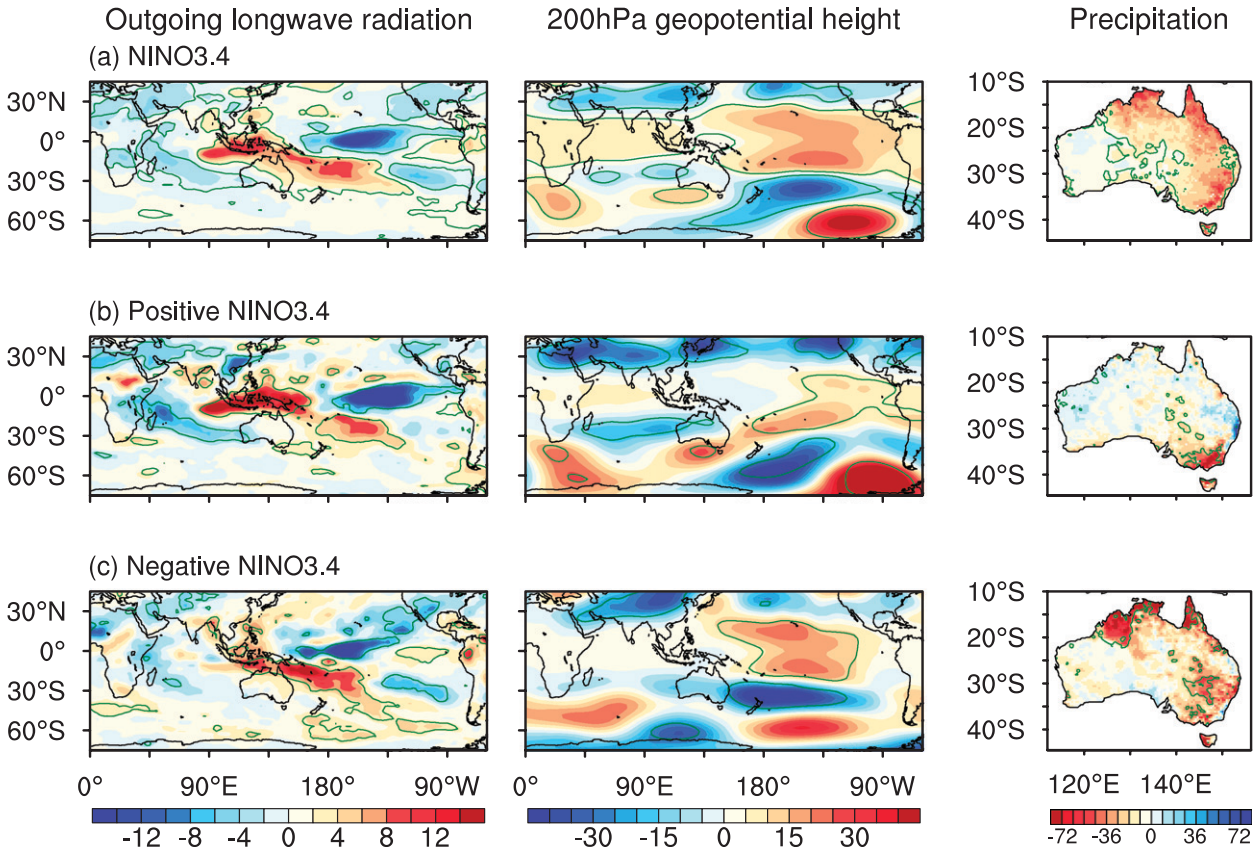

FIG. 2. Circulation anomaly patterns obtained by regressing detrended circulation anomalies onto a detrended Niño-3.4 index using (a) all samples, which implies a linear relationship; (b) samples with positive Niño-3.4 values (El Niño); and (c) samples with negative Niño-3.4 values (La Niña). The regression coefficients (color) and correlation coefficient (green contours, greater than that required for the 95% confidence level) are plotted. Shown are the coefficients associated with OLR (left, W m^{-2} $°C^{-1}$), 200-hPa geopotential height (middle, m $°C^{-1}$), and Australian rainfall (mm SON^{-1}, $°C^{-1}$).

4. Evidence of an asymmetry in the IOD impact

In a linear framework many of the features associated with the IOD are similar to those associated with ENSO, as expected from the high ENSO–IOD coherence (Fig. 3a, compared to Fig. 2a, left to right). While the OLR patterns associated with the IOD are quite similar to those associated with ENSO, notable differences exist, including weaker height anomalies over the tropics, and stronger EIO and WIO wave trains. The high pressure anomaly south of Australia is stronger with a more pronounced response in southeastern Australia rainfall. This rainfall signal stretches across much of southern Australia, with a considerably stronger impact over southwest Western Australia than that seen in the ENSO-induced pattern (Fig. 2a). The larger rainfall response over southern Australian regions occurs as a result of the stronger high pressure (height) anomaly to the south of Australia because of the inclusion of IOD events independent from ENSO.

We now focus on asymmetry with respect to pIOD and nIOD events. Circulation anomalies associated with pIODs (Fig. 3b) are better defined than those associated with nIODs (Fig. 3c). This is evident by the presence of stronger OLR anomalies over the tropics, with corresponding well-defined extratropical wave train patterns associated with pIOD events. In fact, much of the wave train pattern obtained using all samples (Fig. 3a) is contributed by pIOD events (Fig. 3b). There is virtually no such signal in anomaly patterns associated with nIOD events (Fig. 3c). This asymmetry translates into a direct influence on southern Australian rainfall: a reduction in rainfall over southwest Western Australia and southeast Australia systematically increases with a greater pIOD amplitude (Fig. 3b). By contrast, rainfall across the same regions, by and large, does not increase with a stronger nIOD (Fig. 3c).

Despite the high El Niño–pIOD coherence, differences exist between anomaly patterns associated with El Niño and pIOD conditions. First, wave train patterns

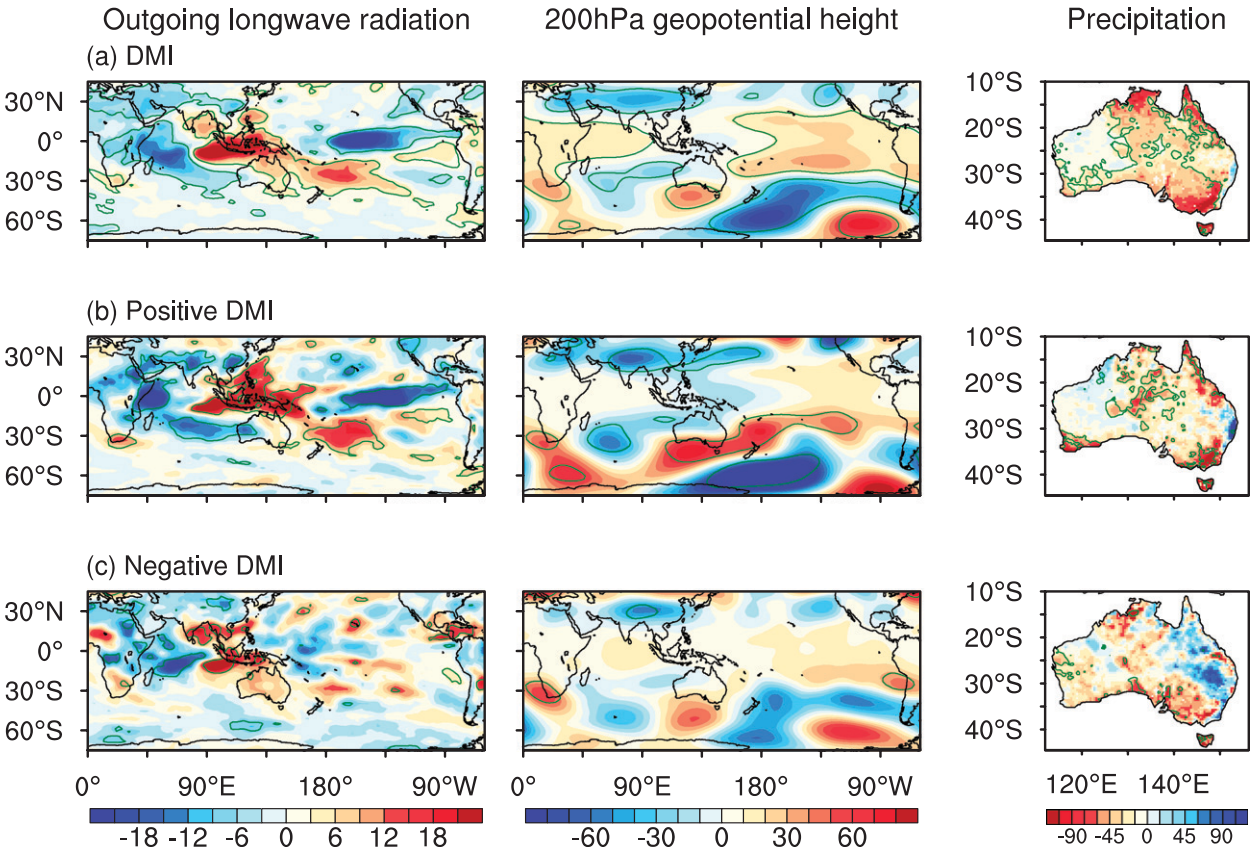

FIG. 3. As in Fig. 2, but using DMI instead of Niño-3.4.

associated with a pIOD are far broader in size and stronger in magnitude, extending the impact to regions such as southwest Western Australia and southern Tasmania, where an impact of El Niño on these regions is not evident (cf. Figs. 2b and 3b, middle panels). Second, a pIOD impact on northern Australia is seen in the convection and rainfall patterns, suggesting that a pIOD exerts an influence on the western pole of the SO as suggested in previous studies (Behera et al. 2006; Luo et al. 2010).

5. Dynamics of the IOD and ENSO impact asymmetry

The amplitude asymmetry of ENSO and the IOD is an important factor underpinning the asymmetry in rainfall impacts. It is well known that there is a positive skewness of ENSO, such that the amplitude of El Niño is greater than that of La Niña. The associated dynamics are still inconclusive, but several mechanisms have been suggested, including oceanic nonlinear dynamical heating (Jin et al. 2003; An and Jin 2004), a nonlinear dependence of tropical deep atmospheric convection to underlying SSTs (Hoerling et al. 1997) (see also Figs. 2b and 2c), and a nonlinear response of zonal wind to equal strength but opposing SST anomalies (Kang and Kug 2002). The positive skewness of ENSO will lead to a greater impact from El Niños because of their larger amplitude compared to La Niñas. This means the impact of El Niño events are better able to emerge from stochastic noise when compared to the impact of La Niña events.

Switching to the TIO, one possible reason for the IODs' asymmetric impacts could be the asymmetric response of Rossby wave trains to their source, that is, anomalous divergence induced by tropical convection anomalies in the TIO. To explore this possibility, we examine the response of extratropical 200-hPa heights (e.g., over south of Australia, 45°–36°S, 116°–138°E) to anomalous divergence over the IODE region. We find that no such asymmetry exists: a statistical relationship is present only when all samples are used (Fig. 4).

It follows that the skewness in the IOD presents a main cause for its asymmetric impacts. What then causes the IOD skewness? Given the strong El Niño–pIOD coherence, the positive skewness of ENSO may

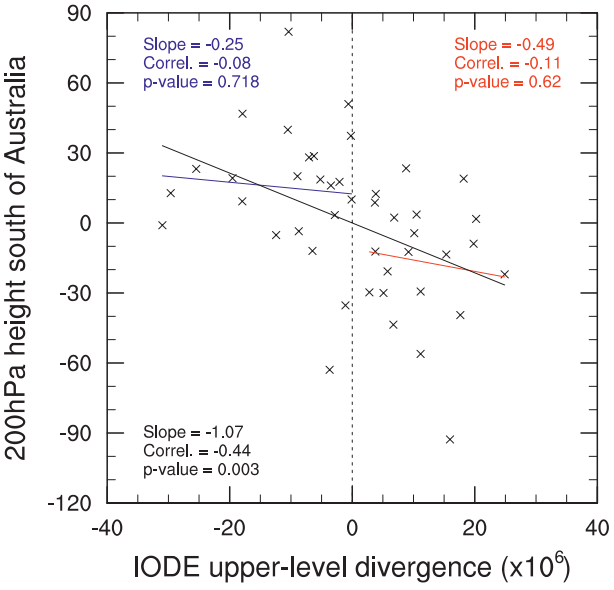

FIG. 4. Scatterplot of the 200-hPa geopotential height anomalies south of Australia (45°–36°S, 116°–138°E) vs upper-level (0.2101 sigma) anomalous divergence over the IODE region during SON over 1958–2001 (a period during which data are available). Three sets of linear regressions are shown, using samples showing anomalous divergence (black), divergent (red), and convergent (blue) flow over the IODE region. The slope, correlation, and *p* value are also shown. Note the divergence has been scaled.

contribute to the positive skewness of the IOD. Linearly removing Niño-3.4 (ENSO) from the DMI (IOD) during SON reduces the DMI skewness from 0.75 to 0.41, falling below significant levels. However, Fig. 1a shows a distinct nonlinear relationship between the IOD and ENSO, which must be taken into account when removing one from the other. Removing ENSO from the IOD in a quadratic manner increases the IOD skewness to 0.81, mainly due to one event in 1961. Another study, Hong et al. (2008), suggests that the IOD skewness is not solely induced by the positive ENSO skewness, because removal of concurrent ENSO events only marginally reduces the IOD eastern pole skewness value. Several possible mechanisms have been proposed to explain the IOD skewness through its internal properties, including a nonlinear dynamic heating for the IODE SST, an asymmetry of the SST–cloud–radiation feedback (Hong et al. 2008), and an asymmetric thermocline–SST feedback (Zheng et al. 2010). During pIOD events, nonlinear zonal and vertical advection reinforce the development of negative IODE SST anomalies, but they act to damp positive IODE SST anomalies, similar to the nonlinear dynamical heating in the Pacific that contributes to a positive skewness of ENSO. Despite the strong consensus on the importance of this feedback, the role of the other two nonlinear processes in the skewness remains controversial.

A breakdown of a SST–cloud–radiation feedback is thought to play a dominant role (Hong et al. 2008). In this negative feedback process, a cold SST anomaly leads to a reduction in cloud amount that causes an increase in net downward shortwave radiation, which in turn suppresses the development of the cold SST anomaly (Ramanathan and Collins 1991; Li et al. 2000). Hong and Li (2010) suggest that for warm IODE SST anomalies, this feedback (damping) can continue in an unhindered manner, with the increase of warm SST anomalies leading to an increase in convection and cloud amount, causing a decrease in the shortwave radiation reaching the surface. However, the same negative feedback works only when the amplitude of cold IODE SST anomalies is small; upon reaching a threshold value, the SST anomalies may completely suppress the mean convection, resulting in cloud-free conditions, upon which point, further cooling is not subject to any damping (Hong et al. 2008). Thereafter, cool SST anomalies are able to grow ''freely'' due to the lack of a thermal damping, a process by which the IOD asymmetry can be generated.

The other mechanism is an asymmetric thermocline–SST feedback: as the mean thermocline in the IODE region is deep, a shoaling thermocline is more effective in inducing a surface cooling than a deepening thermocline that causes a surface warming. For the same one unit of change of the thermocline, the size of a surface cooling is far greater when the thermocline is shoaling than the size of warming when the thermocline is deepening. Zheng et al. (2010) suggest that the asymmetric thermocline–SST feedback is a key process responsible for the negative SST skewness in the IODE. However, Hong and Li (2010) argue that the asymmetric thermocline–SST feedback can be accounted for by the breakdown of the SST–cloud–radiation feedback by showing that there is little asymmetry in the thermocline–subsurface temperature feedback or in the response of equatorial easterly winds to the thermocline.

The asymmetry in the OLR regression coefficients (Figs. 3b and 3c) suggests a completely different mechanism to the breakdown of the SST–cloud–radiation feedback. Our result suggests that the SST–cloud–radiation feedback strengthens in response to increasing cold IODE SST anomalies, with a greater response of the positive OLR. In other words, strong cold SST anomalies develop despite a stronger damping. This is completely opposite to the result of Hong and Li (2010) and deserves a detailed examination.

Figure 5 plots the relationship between SST (from HadISST) and rainfall from NCEP, ERA-40, and GPCP

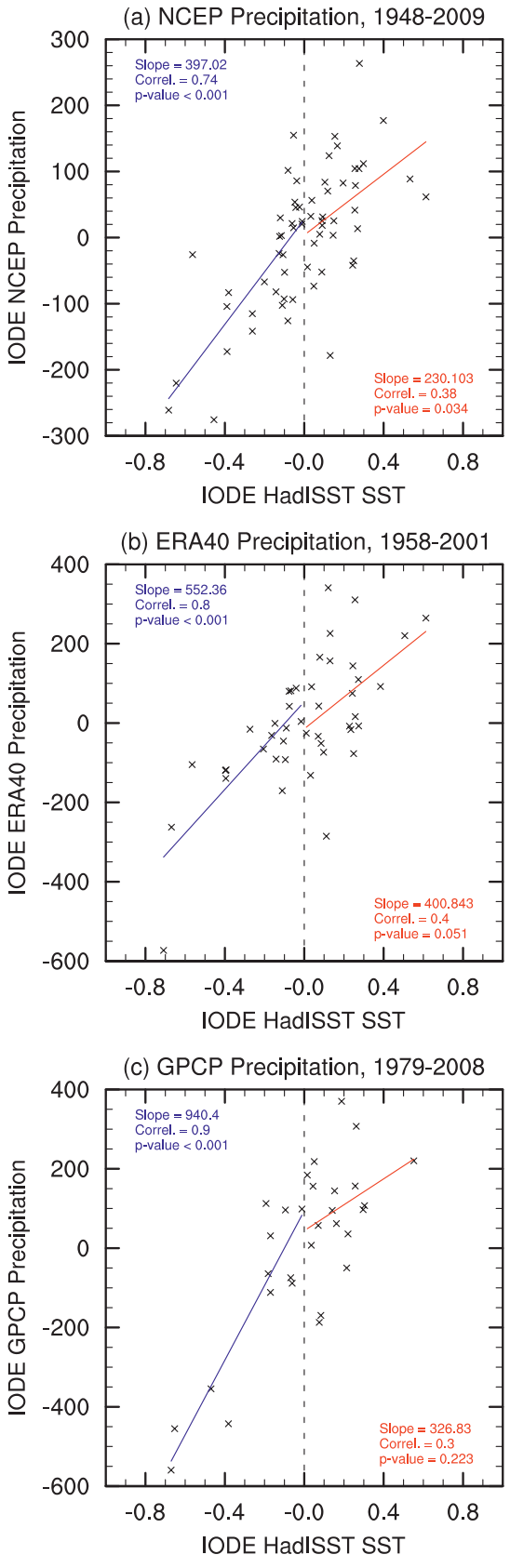

averaged over the IODE region. There is a consistent asymmetry in OLR and shortwave radiation in this region as expected (figures not shown). This is already implied in the OLR patterns using NCEP data (Figs. 3b and 3c). In all three rainfall datasets, an opposite asymmetry is produced to that shown in Fig. 3a of Hong and Li (2010), although the magnitude of the asymmetry is smallest in ERA-40, the dataset used by Hong and Li (2010). It should be noted that Hong and Li (2010) did not detrend their rainfall and temperature samples (from ERA-40 and SODA v2.0.2) before undertaking their analysis. Further discrepancies lie in their SST: they take the SODA temperature at the middepth of model level 1 (5 m) as representing SST and using three pairs of monthly values per season to increase their sample size (increasing the degrees of freedom). In addition to this, Hong and Li (2010) only show samples from the positive and negative quadrants of both rainfall and SST anomalies. An analysis using all monthly raw (undetrended) samples of seasonal SODA SST and ERA-40 rainfall anomalies, divided into positive and negative SST phases does produce a similar asymmetry (Fig. 6a) to that in Hong and Li (2010), with a slope ratio for the positive to negative phases of 2.26:1.

However, when we replace the SODA SST anomalies with HadISST anomalies, the asymmetry shown in Fig. 6a is not evident (Fig. 6b), suggesting that the result of Hong and Li (2010) may be a consequence of the SODA SST biases. A further examination reveals that although warm anomalies from SODA SST and HadISST are comparable (Fig. 6c), negative SST anomalies from SODA are systematically cooler than HadISST negative anomalies. For a 0.6°C cooling in HadISST, there is a 1°C cooling in SODA surface temperature, and so given the large biases in SODA temperatures, the validity of its use in assessing the thermocline–SST feedback is questionable.

Another factor is a strong increasing trend in ERA-40 rainfall over the IODE region, which is virtually absent in the GPCP and NCEP rainfall (Fig. 7). The positive rainfall trend from ERA-40 skews the samples toward large positive rainfall anomalies that boost the slope to

←

FIG. 5. Scatterplot of linearly detrended SON rainfall anomalies averaged over the IODE region from (a) NCEP (1948–2009), (b) ERA-40 (1958–2001), and (c) GPCP (1979–2008) vs detrended SST anomalies averaged over the IODE region. Two sets of linear regressions are shown, using samples with a positive IODE SST (red) and a negative IODE SST (blue). The slope, correlation, and *p* value are also shown.

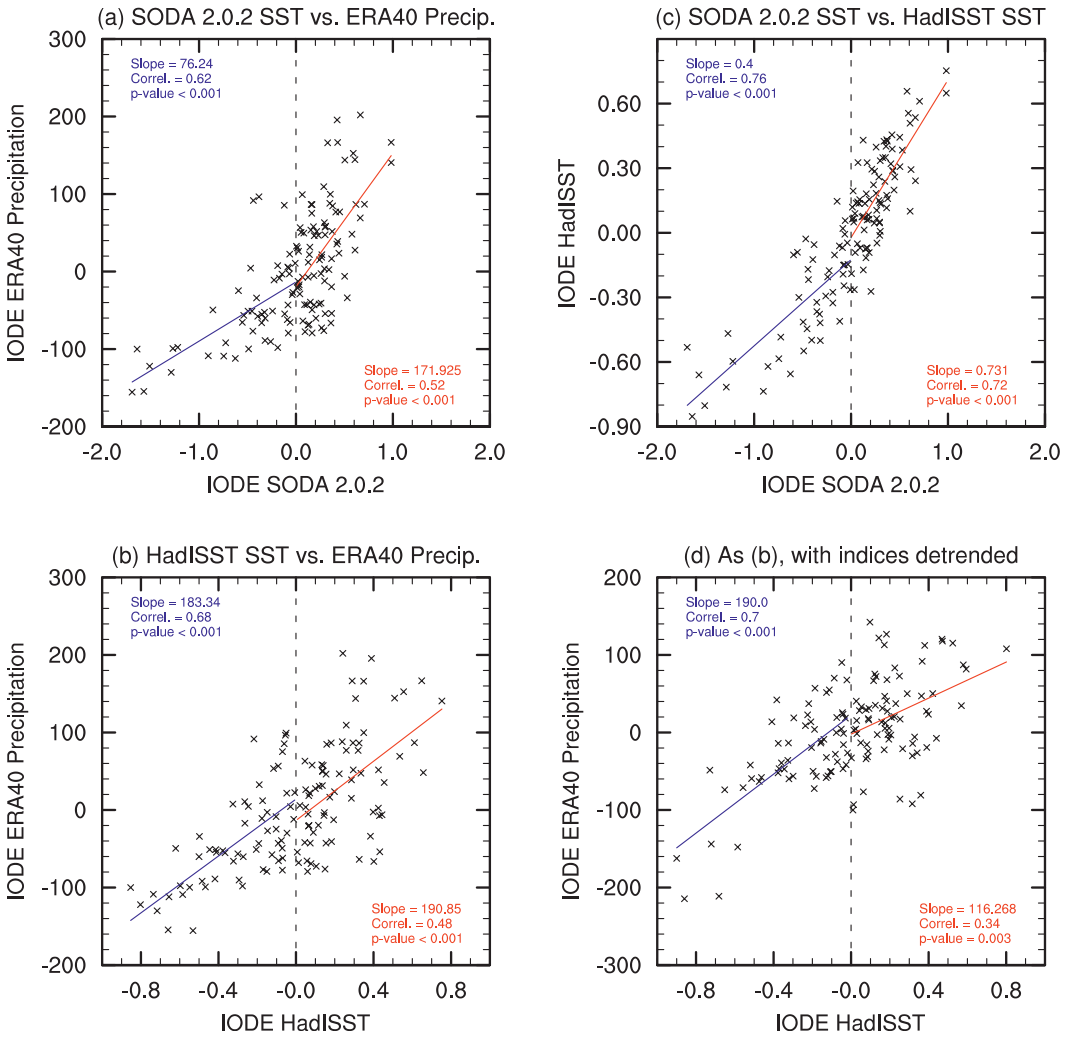

FIG. 6. Scatterplot of (a) monthly raw rainfall anomalies averaged over the IODE region from ERA-40 vs monthly raw IODE SST anomalies from SODA [three pairs per each SON, as from Hong and Li (2010)]. (b) As in (a), but replacing SODA IODE SST anomalies with raw HadISST IODE SST anomalies. (c) Monthly raw HadISST IODE SST anomalies vs monthly SODA IODE SST anomalies. (d) As in (b), but using linearly detrended data. Two sets of linear regression are shown, including samples with a positive IODE SST (red) and a negative IODE SST (blue). The slope, correlation, and p value are also shown.

the warm IODE SST domain (Fig. 6a). Once the rainfall time series is detrended, the asymmetry becomes opposite to that shown by Hong and Li (2010) (Fig. 6d), consistent with the results using different rainfall and SST datasets (Figs. 5a–c). Thus, the bias in SODA SST combined with an unrealistic trend in ERA-40 rainfall leads to the false impression of a breakdown in the SST–cloud–radiation negative feedback.

In fact, a possibility exists that a breakdown in SST–cloud–radiation feedback may contribute to a negative IOD skewness (or positive skewness in the IODE SST). That is, upon reaching a threshold value, warm SST anomalies may not increase cloud, upon which point further warming is not subject to any damping, leading to a large amplitude of positive SST anomalies over the eastern pole. However, an examination of daily clouds from NCEP shows no occurrences of days with a 100% cloud cover. Likewise, there are no occurrences of days with clear sky, indicating a breakdown of this feedback process in either positive or negative SST rarely occurs.

6. Discussion and conclusions

Using a typical linear regression/correlation framework, the impact pathway of ENSO and the IOD has previously been assumed to be symmetric with respect

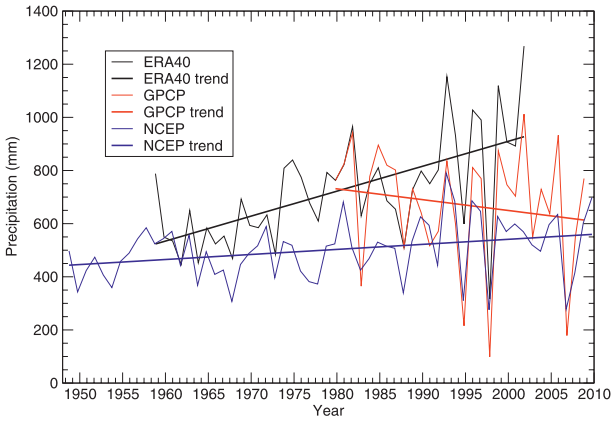

FIG. 7. Time series of SON rainfall averaged over the IODE region from ERA-40 (1958–2001), GPCP (1979–2008), and NCEP (1948–2009). A linear trend line is superimposed for all three time series.

to the combined positive and negative phases of these modes. Using such an approach, Cai et al. (2011) show that in austral spring the impact of ENSO on extratropical regions such as southern Australia is conducted via the TIO, through its strong coherence with the IOD. The associated convection anomalies in the TIO act as a source of EIO and WIO equivalent barotropic stationary Rossby wave trains. The wave trains share a pressure/height anomaly south of Australia, whereby, weather systems that deliver rain to southern and southeastern Australia are reduced. The analysis, however, assumes linearity. The present study shows that a strong asymmetry does in fact exist in the impact of ENSO and the IOD.

A major contribution of the present study is the identification of an asymmetry in the impact of El Niño and La Niña events, and in the impact of pIOD and nIOD events in terms of an extratropical response. We find that the extratropical circulation response delivered via TIO Rossby wave trains occurs primarily during El Niño and pIOD events. A schematic is presented in Fig. 8, which is a modification of Fig. 9c in Cai et al. (2011) for SON. A pIOD impact on extratropical circulation via excitation of Indian Ocean wave trains operates regardless of whether there is a coherent El Niño, but an impact of El Niño is conducted through a coherent pIOD via these wave trains because the PSA is too far east of Australia (Fig. 8a). During nIOD events, the Indian Ocean wave train response is far weaker, and less well defined (Fig. 8b, indicated by a dashed arrow).

A further contribution is the characterization of the asymmetrical ENSO impact in regions such as southern Australia. In terms of the tropical response, during La Niña, northern Australia (north of 22°S) experiences increased rainfall associated with enhanced convection

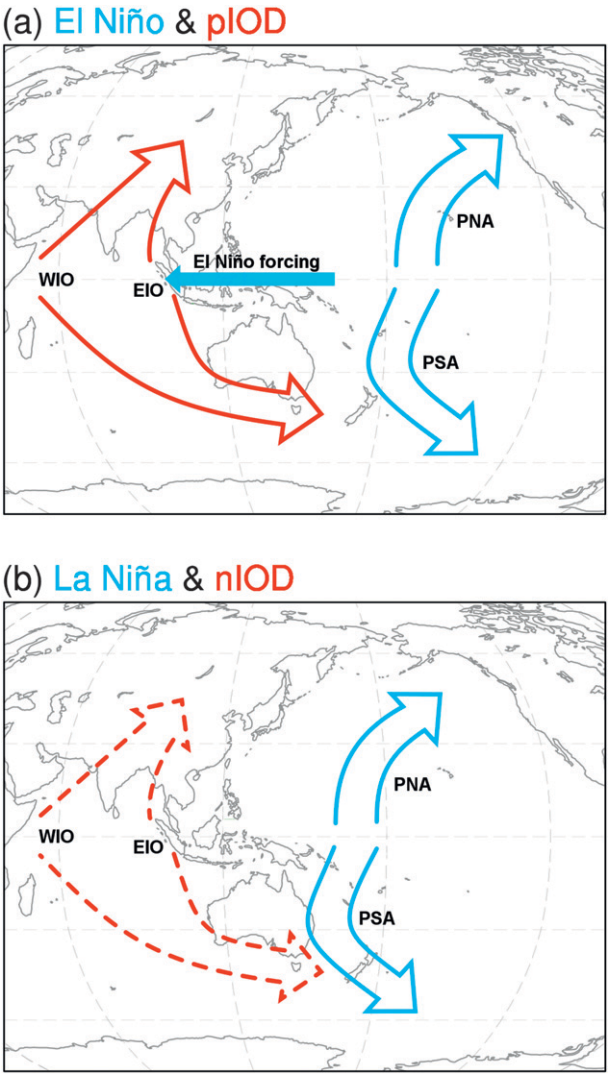

FIG. 8. Schematic of the teleconnective pathways of (a) El Niño and pIOD, and (b) La Niña and nIOD. The dashed arrows indicate a teleconnection pathway that is not significant. The impact from the pIOD is greater than that from nIOD, and is delivered through the WIO and EIO wave trains. The impact of El Niño on some extratropical regions (including southern Australia) is conducted through coherence with a pIOD. However, the impact of La Niña on southern Australia is not delivered through TIO but through the PSA pattern, which is located closer to Australia than during El Niño.

over the west Pacific; however, during El Niño little influence on rainfall is seen because the maximum convection anomalies occur in the central Pacific. In terms of the extratropical response, although El Niño conducts its teleconnective impact on southern Australia through the TIO, La Niña is able to conduct its impact on parts of eastern Australia (between 27° and 35°S) via the PSA pattern (illustrated by comparing Figs. 8a and 8b). Tropical convection anomalies associated with La Niña

are located in the west Pacific, leading to a PSA-induced low pressure anomaly situated closer to Australia, enhancing the rain-bearing easterly weather systems. These asymmetries in the regional impact help explain the ENSO–Australian rainfall teleconnection pattern (right panel, Fig. 2a); in particular, they provide an explanation for the lack of an ENSO-induced rainfall signal over the 22°–27°S latitude band of eastern Australia, as this region marks the separation of the tropical from the extratropical response.

Contributing to this asymmetry is a strong positive skewness in ENSO and the IOD. Although the dynamics for the skewness are not well understood, the presence has been well documented. The greater amplitude of pIOD and El Niño events means that the response in atmospheric circulation anomalies is better manifested out of stochastic noise, giving a more well-defined stronger response and impact.

Another contribution of the present study is the debate concerning the dynamics of the IOD skewness. Proposed mechanisms for this skewness range from nonlinear processes such as dynamical heating, a SST–cloud–radiation feedback (Hong et al. 2008), and a thermocline–SST feedback (Zheng et al. 2010) in the IODE region. We demonstrate that the IOD skewness occurs not because of a breakdown in the SST–cloud–radiation feedback, but despite the damping effect from this feedback. In fact, the presence of a stronger pIOD impact with a better-defined wave train pattern constitutes direct evidence that the breakdown of SST–cloud–radiation feedback is not a contributing factor to the IOD skewness. It infers that the IOD amplitude asymmetry is caused by other feedbacks, such as the nonlinear thermocline–SST feedback and the nonlinear dynamical heating. A reassessment of their relative importance is therefore needed.

The presence of the IOD impact asymmetry on the extratropical climate implies that the impact of ENSO via the TIO wave trains is asymmetric, even if ENSO properties and the IOD–ENSO coherence are symmetric. The asymmetry in ENSO's impact is enhanced by a stronger pIOD–El Niño coherence than that of nIOD–La Niña, and a positive skewness of ENSO. It is not clear to what extent the stronger El Niño–pIOD coherence is a consequence of a positive skewness in both ENSO and the IOD, as they are able to force each other. What is clear is that the dynamics reside at least in part in their respective ocean basins.

Finally, our results indicate that pIOD events have a stronger impact on southern Australia than nIOD events. This provides a framework for interpreting the recent spring drying trend over southeast Australia, a region strongly affected by the IOD (Figs. 2b and 3b) (Cai et al. 2009a,b). Since the 1950s, spring rainfall across southeast Australia has experienced a reduction of around 30 mm (Cai et al. 2009b). Leading into the dry summer season (December–February), a spring rainfall reduction has a widespread impact on catchment inflows across the Murray–Darling basin, and increases the likelihood of severe bushfire occurrences. For example, more than half of major summer bushfires over southeast Australia are preceded by a pIOD event in the prior spring season (Cai et al. 2009a). Over the past decades, the frequency of pIODs has been unprecedentedly high, whereas the frequency of nIOD occurrences is at a historically low level (Cai et al. 2009b). These studies suggest that it is the high frequency of pIOD events, heightened by three consecutive events from 2006 to 2008 (Cai et al. 2009d) that contributes to the recent spring rainfall decline across southeast Australia. An alternative explanation for the recent decline is a lack of nIOD events (Ummenhofer et al. 2009). While either an increase in pIOD events or a reduction in nIOD occurrences will contribute to a spring rainfall reduction, our result suggests that an increased pIOD frequency is far more effective in generating a spring rainfall reduction over southeast Australia.

Acknowledgments. This research is supported by the Australian Climate Change Science Program (ACCSP), South Eastearn Australian Climate Initiative (SEACI), the Western Australian Marine Science Institution (WAMSI), the Goyder Institute, and the Grains Research and Development Corporation (GRDC). The authors wish to thank three anonymous reviewers for their useful comments.

REFERENCES

Adler, R. F., and Coauthors, 2003: The Version-2 Global Precipitation Climatology Project (GPCP) monthly precipitation analysis (1979–present). *J. Hydrometeor.,* **4,** 1147–1167.

An, S.-I., and F.-F. Jin, 2004: Nonlinearity and asymmetry of ENSO. *J. Climate,* **17,** 2399–2412.

Ashok, K., S. K. Behera, S. A. Rao, H. Weng, and T. Yamagata, 2007: El Niño Modoki and its possible teleconnection. *J. Geophys. Res.,* **112,** C11007, doi:10.1029/2006JC003798.

Behera, S. K., J. J. Luo, S. Masson, S. A. Rao, H. Sakuma, and T. Yamagata, 2006: A CGCM study on the interaction between IOD and ENSO. *J. Climate,* **19,** 1688–1705.

Burgers, G., and D. B. Stephenson, 1999: The ''normality'' of El Niño. *Geophys. Res. Lett.,* **26,** 1027–1030.

Cai, W., T. Cowan, and M. Raupach, 2009a: Positive Indian Ocean dipole events precondition southeast Australia bushfires. *Geophys. Res. Lett.,* **36,** L19710, doi:10.1029/2009GL039902.

——, ——, and A. Sullivan, 2009b: Recent unprecedented skewness towards positive Indian Ocean dipole occurrences and its impact on Australian rainfall. *Geophys. Res. Lett.,* **36,** L11705, doi:10.1029/2009GL037604.

——, A. Pan, D. Roemmich, T. Cowan, and X. Guo, 2009c: Argo profiles a rare occurrence of three consecutive positive Indian Ocean dipole events, 2006–2008. *Geophys. Res. Lett.,* **36,** L08701, doi:10.1029/2008GL037038.

——, A. Sullivan, and T. Cowan, 2009d: How rare are the 2006–2008 positive Indian Ocean dipole events? An IPCC AR4 climate model perspective. *Geophys. Res. Lett.,* **36,** L08702, doi:10.1029/2009GL037982.

——, P. van Rensch, T. Cowan, and H. H. Hendon, 2011: Teleconnection pathways of ENSO and the IOD and the mechanisms for impacts on Australian rainfall. *J. Climate,* **24,** 3910–3923.

Carton, J. A., and B. S. Giese, 2008: A reanalysis of ocean climate using Simple Ocean Data Assimilation (SODA). *Mon. Wea. Rev.,* **136,** 2999–3017.

Chan, S. C., S. K. Behera, and T. Yamagata, 2008: Indian Ocean dipole influence on South American rainfall. *Geophys. Res. Lett.,* **35,** L14S12, doi:10.1029/2008GL034204.

Gill, A. E., 1980: Some simple solutions for heat-induced tropical circulation. *Quart. J. Roy. Meteor. Soc.,* **106,** 447–462.

Hoerling, M. P., A. Kumar, and M. Zhong, 1997: El Niño, La Niña, and the nonlinearity of their teleconnections. *J. Climate,* **10,** 1769–1786.

Hong, C.-C., and T. Li, 2010: Independence of SST skewness from thermocline feedback in the eastern equatorial Indian Ocean. *Geophys. Res. Lett.,* **37,** L11702, doi:10.1029/2010GL043380.

——, ——, H. Lin, and J. S. Kug, 2008: Asymmetry of the Indian Ocean dipole. Part I: Observational analysis. *J. Climate,* **21,** 4834–4848.

Hoskins, B. J., and D. J. Karoly, 1981: The steady linear response of a spherical atmosphere to thermal and orographic forcing. *J. Atmos. Sci.,* **38,** 1179–1196.

Jin, F.-F., S.-I. An, A. Timmermann, and J. Zhao, 2003: Strong El Niño events and nonlinear dynamical heating. *Geophys. Res. Lett.,* **30,** 1120, doi:10.1029/2002GL016356.

Jones, D. A., W. Wang, and R. Fawcett, 2009: High-quality spatial climate data-sets for Australia. *Aust. Meteor. Oceanogr. J.,* **58,** 233–248.

Kalnay, E., and Coauthors, 1996: The NCEP/NCAR 40-Year Reanalysis Project. *Bull. Amer. Meteor. Soc.,* **77,** 437–471.

Kang, I.-S., and J.-S. Kug, 2002: El Niño and La Niña sea surface temperature anomalies: Asymmetry characteristics associated with their wind stress anomalies. *J. Geophys. Res.,* **107,** 4372, doi:10.1029/2001JD000393.

Kug, J.-S., and I.-S. Kang, 2006: Interactive feedback between ENSO and the Indian Ocean. *J. Climate,* **19,** 1784–1801.

Li, T., T. F. Hogan, and C. P. Chang, 2000: Dynamic and thermodynamic regulation of ocean warming. *J. Atmos. Sci.,* **57,** 3353–3365.

——, B. Wang, C.-P. Chang, and Y. Zhang, 2003: A theory for the Indian Ocean dipole–zonal mode. *J. Atmos. Sci.,* **60,** 2119–2135.

Luo, J.-J., R. Zhang, S. K. Behera, Y. Masumoto, F.-F. Jin, R. Lukas, and T. Yamagata, 2010: Interaction between El Niño and extreme Indian Ocean dipole. *J. Climate,* **23,** 726–742.

Newman, M., P. D. Sardeshmukh, and J. W. Bergman, 2000: An assessment of the NCEP, NASA, and ECMWF reanalysis over the tropical west Pacific warm pool. *Bull. Amer. Meteor. Soc.,* **81,** 41–48.

Ramanathan, V., and W. Collins, 1991: Thermodynamic regulation of ocean warming by cirrus clouds deduced from observations of the 1987 El Niño. *Nature,* **351,** 27–32.

Rayner, N. A., D. E. Parker, E. B. Horton, C. K. Folland, L. V. Alexander, D. P. Rowell, E. C. Kent, and A. Kaplan, 2003: Global analyses of sea surface temperature, sea ice, and night marine air temperature since the late nineteenth century. *J. Geophys. Res.,* **108,** 4407, doi:10.1029/2002JD002670.

Ropelewski, C. F., and M. S. Halpert, 1987: Global and regional scale precipitation patterns associated with the El Niño/Southern Oscillation. *Mon. Wea. Rev.,* **115,** 1606–1626.

Saji, N. H., and T. Yamagata, 2003a: Possible impacts of Indian Ocean dipole mode events on global climate. *Climate Res.,* **25,** 151–169.

——, and ——, 2003b: Structure of SST and surface wind variability during Indian Ocean dipole mode events: COADS observations. *J. Climate,* **16,** 2735–2751.

——, B. N. Goswami, P. N. Vinayachandran, and T. Yamagata, 1999: A dipole mode in the tropical Indian Ocean. *Nature,* **401,** 360–363.

Ummenhofer, C. C., M. H. England, P. C. McIntosh, G. A. Meyers, M. J. Pook, J. S. Risbey, A. Sen Gupta, and A. S. Taschetto, 2009: What causes southeast Australia's worst droughts? *Geophys. Res. Lett.,* **36,** L04706, doi:10.1029/2008GL036801.

Zheng, X.-T., S.-P. Xie, G. A. Vecchi, Q. Liu, and J. Hafner, 2010: Indian Ocean dipole response to global warming: Analysis of ocean–atmospheric feedbacks in a coupled model. *J. Climate,* **23,** 1240–1253.